Silkworm cocoons inspire models for random fiber and particulate composites

Fujia Chen, David Porter,* and Fritz Vollrath
Department of Zoology, University of Oxford, Oxford OX1 3PS, United Kingdom
(Received 5 May 2010; revised manuscript received 30 June 2010; published 14 October 2010)

The bioengineering design principles evolved in silkworm cocoons make them ideal natural prototypes and models for structural composites. Cocoons depend for their stiffness and strength on the connectivity of bonding between their constituent materials of silk fibers and sericin binder. Strain-activated mechanisms for loss of bonding connectivity in cocoons can be translated directly into a surprisingly simple yet universal set of physically realistic as well as predictive quantitative structure-property relations for a wide range of technologically important fiber and particulate composite materials.

DOI: 10.1103/PhysRevE.82.041911 PACS number(s): 87.85.jc, 81.05.Ni, 62.20.mm, 12.60.Rc

I. INTRODUCTION

The outstanding mechanical properties of strength and toughness in silks have coevolved with the bioengineering structures in which they serve, such as spider's webs as superb models of light-weight engineering. Silkworm cocoons have evolved over millions of years by a process of natural selection to nurture and protect moths and butterflies in a wide range of different environments and exposed to many different threats and predators [1]. A cocoon is a natural protein polymer composite shell with a nonwoven structure constructed by the animal from a continuous semicrystalline fibroin silk strand with a length of about 1000 m and diameters of 10–30 μm, which is bonded together by about 25% amorphous sericin [2,3]. It has a similar microstructure to other stochastic fibrous materials such as paper, nonwoven textiles, and electrospun polymer mats. Quantitative models for the mechanical properties of cocoons could not be found in the literature. However, since nonwoven fiber materials are technologically very important, there are a number of models for these similar structure materials, particularly paper.

For paper, the semiempirical theory of Page [4] and the mechanistic theory of Kallmes [5] separate the bonding contributions to tensile strength into the influence of the area of interfiber bonds that is bonded to other fibers and that of the shear bond strength per unit area acting in these regions. In a network under strain, the bonded regions of the fiber surfaces facilitate the transfer of stress between fiber segments, and this is the basis of shear-lag theory [6]. Favorable comparisons between Cox's theory and experimental observation have been reported [7–10], but shortcomings of the shear-lag model have been voiced by Raisanen *et al.* [12,13] that the transfer of axial stress in random fiber networks could not be accounted for by the shear-lag approach. Eichhorn and Young [14] observed significant strains at the ends of fibers within the network, contrary to the prediction of Cox that strain would be zero at the fiber ends. I'Anson and Sampson [11] suggested that when a network in which the number of fibers per unit area is just above the percolation threshold fails under a tensile stress, the dominant mechanism of failure will be that of bonds breaking rather than fibers because the number of contacts per fiber is typically insufficient to transfer enough stress to a fiber for it to fail. The strength of paper has also been modeled by scaling test results from small samples using classic Weibull's theory [15–17], which suggests an exponential decrease in the specific strength of a sample with increasing volume as the probability of a "weak link" in the material under investigation increases with increasing volume.

We tried to apply these models to our experimental observations on the mechanical properties of silkworm cocoons but found that the models were mathematically complex and also required numbers of fitting parameters to reproduce the data rather than to predict properties using a limited number of parameters that can be calculated directly from the component material properties and composite morphology. We therefore used our experimental observations on silkworm cocoons, with a first priority to develop a physically realistic model (namely, including all the observed structural effects under deformation) that can quantitatively calculate cocoon properties using a minimum number of material parameters, which themselves can be calculated independently. Our model takes the simple hypothesis that stiffness reduces as the number of bonding sites in a cocoon reduces under increasing load and quantifies this process as loss of connectivity in the composite due to strain-activated bond breaking.

In itself, such a model for silkworm cocoons has limited technological value, and such a bioinspired model needs to be able to predict (rather than just reproduce) the properties of a range of other "synthetic" materials with similar characteristics. The first obvious set of materials to consider were nonwoven random fiber networks for which previous models had been developed but have been found to have the shortcomings outlined above. We then noticed that the simplest form of our model has remarkable similarity to stress-strain profiles of particulate composites. Both of these types of composite can be linked to our model through the loss of connectivity of bonding under load, and so we used a number of such composites as examples to both illustrate and validate our bioinspired model in materials of great technological and economic importance.

II. COCOON STRUCTURE AND PROPERTIES

A cocoon contains a single continuous silk strand with a length of about 1000 m, which is laid down in loops into

*Corresponding author. david.porter@zoo.ox.ac.uk

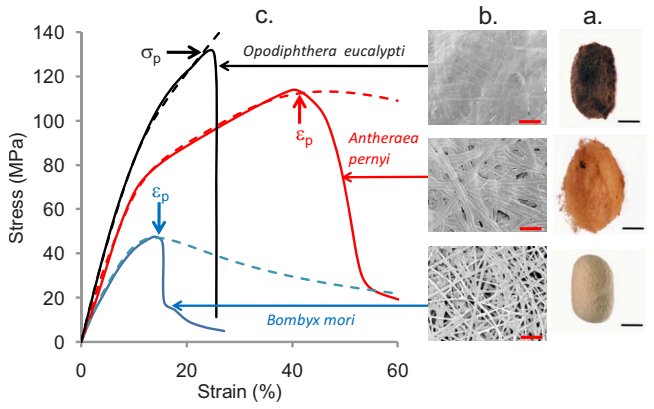

FIG. 1. (Color online) (a) The cocoons of *Bombyx mori*, *Antheraea pernyi*, and *Opodiphthera eucalypti* (scale bar: 10 mm). (b) Typically bonded nonwoven structure of the middle layers of the cocoons (scale bar: 200 μm). (c) Stress-strain profiles for the cocoon walls, with solid lines showing experimental measurements and dashed lines as model calculations, with failure conditions shown as arrows in either stress (σ_p) or strain (ε_p).

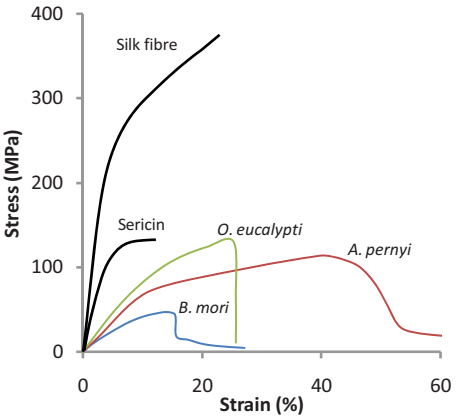

FIG. 2. (Color online) Comparison of the stress-strain profile of the component materials and the example cocoons as labeled.

layers by the gyrating motion of the silkworm head. Each fiber is composed of two fibroin brins conglutinated by a layer of sericin, which can be washed off by different degumming methods in order to reel the silk in the textile industry. Importantly for the argument of "Learning from Nature" [18–21], lepidopteran cocoons look and behave very much like synthetic nonwoven composite materials with mechanical properties that change systematically with features such as porosity and amount of sericin matrix binder.

A multilayer structure has been found in the cocoon. Zhao *et al.* measured the mechanical properties of the cocoon [2,3]. They divided a cocoon into three main layers—innermost layer (pelade), middle layer, and outmost layer—and found that the innermost layer was superior to the corresponding thickness-averaged values of the complete cocoon.

Figure 1 shows overall cocoon structure as well as the central nonwoven network layer morphology of three different moth species (*Bombyx mori*, *Antheraea pernyi*, and *Opodiphthera eucalypti* collected from Worldwide Butterflies, U.K.) alongside measured stress-strain plots (solid lines) for the full cocoon walls, which are good examples of properties at the lower, middle, and upper limits of mechanical properties across a wide range of cocoon types, respectively, from our database of about 35 diverse silkworm types. Stress rises with a reducing modulus as strain increases and the binding points between fibers are observed to break progressively. After a peak stress, there is a rapid fall in stress, indicating a state without a continuous bonded pathway through the sample, which by now is held together simply by entangled fibers. An Instron 5542 instrument was used for the tensile and creep tests. Strips of cocoon wall were cut with dimensions of 5×15 mm with a gauge length of 5 mm and tensile tests were carried out at a speed of 2 mm/min.

Figure 2 shows the stress-strain characteristics of the component silk fiber and sericin materials and the overall cocoons. The component material properties can be measured experimentally or calculated using published structure-property relations [22–24]. For our model, the key generic material parameters are a silk fiber initial tensile modulus $Y_f \approx 9$ GPa and strength of about 400 MPa as well as a sericin matrix modulus of 3.5 GPa and a failure stress of 130 MPa.

We now show that a physically realistic model for nonlinear mechanical properties of the cocoon walls in terms of the component materials and the composite morphology can be derived from those data.

III. CONNECTIVITY MODEL FOR COCOON PROPERTIES

The initial elastic modulus of the cocoon walls, Y, is significantly lower than that of the fibers and binder due to bending of the circular arcs of fiber with a radius of about 2 mm spun by the gyrating silkworms [2,25] and was found to follow the open cell foam model of Zhu *et al.* [26]. This is an extension of the simpler Gibson-Ashby [27] proportionality in density squared and shows how the elastic modulus of the composite is controlled by porosity, where ρ is composite density relative to that of the solid, $\rho_s \approx 1300$ kg m^{-3}. Here,

$$\frac{Y}{Y_f} \approx \frac{2}{3}\left(\frac{\rho}{\rho_s}\right)^2\left(1+\frac{\rho}{\rho_s}\right)^{-1}. \quad (1)$$

Our observations suggest that damage through loss of connectivity of bonding between fibers gradually reduces the stiffness of the composite with increasing strain. Accordingly, we adopt a pragmatic fracture mechanics approach and scale modulus linearly with the active fraction of bonded fibers that sustains load. In this radically simple connectivity model, we quantify the fraction of broken bonds by using an Arrhenius activation function in mechanical energy of deformation in strain, ε, relative to an activation strain, ε_a, squared, since elastic energy density is proportional to elastic strain squared.

Assuming a number of different activation effects, i.e., with fractional contribution f_i the relation for stress, σ, with initial composite modulus, Y, becomes

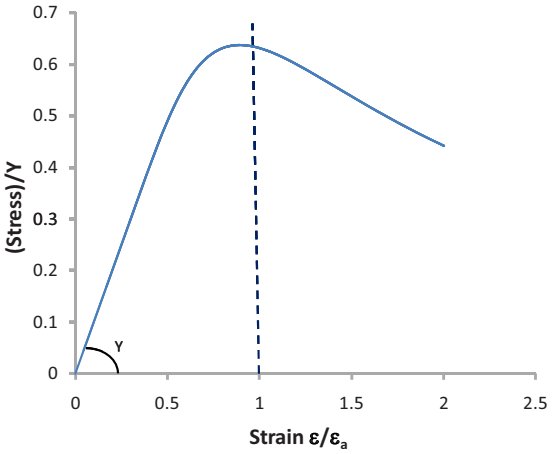

FIG. 3. (Color online) Simplest model normalized stress-strain profile for a single-component contribution of Eq. (2) with an activation strain, $\varepsilon_a=1$, and initial modulus, $Y=1$, showing how damage to the materials and bonding through ε_a lead to loss of stiffness.

$$\sigma = Y\varepsilon\left\{1 - \sum_i f_i \exp\left[-\left(\frac{\varepsilon_{ai}}{\varepsilon}\right)^2\right]\right\}, \quad \text{where } f_i = \frac{Y_i}{Y} \quad (2)$$

and the normalized ($\varepsilon_a=1$, $Y=1$) stress contribution of a single fraction is shown in Fig. 3 to illustrate the relation.

The typical three-layer morphology of cocoons of outer, central, and inner [2,3] first led us to expect three different activated bond breaking effects to be associated with the different binder concentrations in layers. However, a more detailed analysis of further cocoon types and their component layers demonstrated that the three different activated processes are associated with the component materials and bonding morphology.

The model parameters used to fit the cocoons and the example composite materials of the paper are given in Table I.

The first two sets of mechanical parameters, $i=1$ and 2, are the same for all the cocoons and are the activation strains, ε_{ai}, and the "modulus" Y_i of the sericin and the fiber contributions, respectively: $\varepsilon_{a1}=0.06$, $\varepsilon_{a2}=0.16$, $Y_1=130$ MPa, and $Y_2=425$ MPa. Rather than being a classical elastic modulus, Y_i is identical with the failure stress of each material as it degrades under increasing strain effectively at constant load and ε_{ai} is characteristic of the breaking strain of each material. The third parameter set, $i=3$, is associated with the uncoiling of the morphology as the interfiber bonding is broken. The activation strain for uncoiling or straightening of a semicircular arc is $\varepsilon_{a3}\approx 0.6$ for all the cocoons. Since models such as that of Zhu in Eq. (1) allow calculation of the initial cocoon modulus and Y_1 and Y_2 are known, the final model parameter $Y_3=Y-(Y_1+Y_2)$.

Thus, all the parameters for Eq. (2) can be calculated directly from the cocoon structure and model predictions (dashed lines) are compared with observation (solid lines) in Fig. 1. The important differentiating parameter is M_3, which increases to the limiting value of fiber strength of about 400 MPa as the amount of interfiber bonding increases and more fiber sustains load directly.

The model provides important insights into how structural changes with increasing strain control properties. Equation (2) gives us the fraction of elastically active material (in parenthesis) at any strain relative to ε_a, which gives the recoverable strain, ε_r, as the material relaxes back from any applied total strain, ε. Ignoring nonlinear viscoelastic relaxation rate effects in this initial treatment, we can thus calculate the cyclical loading of cocoon wall for *A. pernyi* [shown in Fig. 4(a)], where applied strain is increased in 10% increments and then relaxed back to zero stress through σ_r. The recoverable stress and strain is taken here to be linear with a modulus Y_r given by σ_r/ε_r at any point below an applied total strain. Once that strain has been exceeded and more cumulative damage develops, the recoverable strain again follows the overall envelop. The observed cyclical response is shown in Fig. 4(b) for comparison and includes more complex viscoelastic relaxation effects. However, the trends are well reproduced by the model.

Importantly, we see that failure is rapid after a critical strain, above which there appears to be no continuous bonding path to sustain load. This condition was found to correspond to the stress-strain point where $Y_r\approx Y/2$ as a bond percolation condition [28] or (for *O. eucalypti*, for example) the failure stress of the weaker sericin binder component at about 130 MPa, whichever is the lower. This condition is marked in Fig. 1 as ε_p or σ_p for the three cocoons and agrees

TABLE I. Parameters for the cocoon model and other examples.

Material	ε_{ai}			Y_i (MPa)		
i	1	2	3	1	2	3
Bombyx mori	0.05	0.16	0.6	130	425	10
Antheraea pernyi	0.05	0.16	0.6	130	425	240
Opodiphthera eucalypti	0.05	0.16	0.6	130	425	400
Nonwoven cloth	0.06	0.23		260	260	
Paper	0.025	0.077		700	700	
Nanomat		0.11	0.7		40	40
PBX (at 1 s^{-1})	0.033			900		
Concrete (compression)	0.0025			12200		

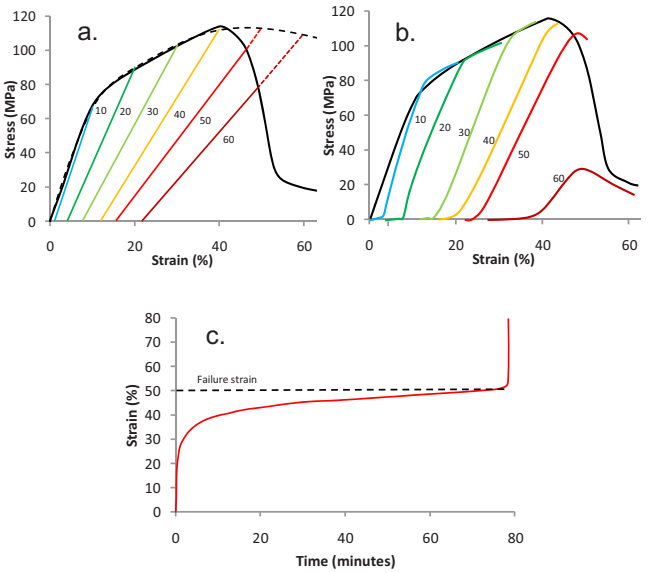

FIG. 4. (Color online) Demonstration that strain is the key activation parameter for damage effects on mechanical properties using recoverable elastic and plastic strain effects in *A. pernyi* cocoons. (a) Predicted recoverable elastic strain after deformation to a given total strain, as labeled. (b) Measured recoverable strain to the same series of total strains as in (a). (c) Evolution of strain with time in a creep experiment after an initial elastic strain of 18%, showing the cocoon fails at a relatively constant value of strain.

well with observation. A general plot of the predicted failure conditions of percolation strain and failure stress are shown in Fig. 5 as dashed lines superimposed upon the predicted stress-strain profiles of cocoon with different values of Y_3 as marked.

That strain appears to be the dominant activation parameter for bond breaking and hence for mechanical properties is shown by examination of stress relaxation and time dependence of creep strain under constant load. Figure 4(c) shows strain as a function of time under a constant stress of about 80 MPa for *A. pernyi*, where strain increases with an exponential relaxation form from the short-time elastic value of 18% with a relaxation time of 150 s, and the sample breaks

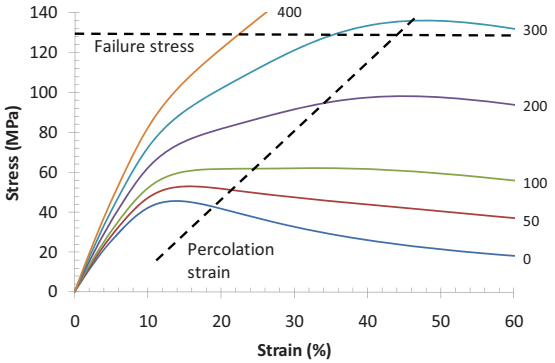

FIG. 5. (Color online) Predicted stress-strain profiles of cocoons with different values of the parameter Y_3 (marked), with predicted failure criteria of stress and percolation strain shown as dashed lines.

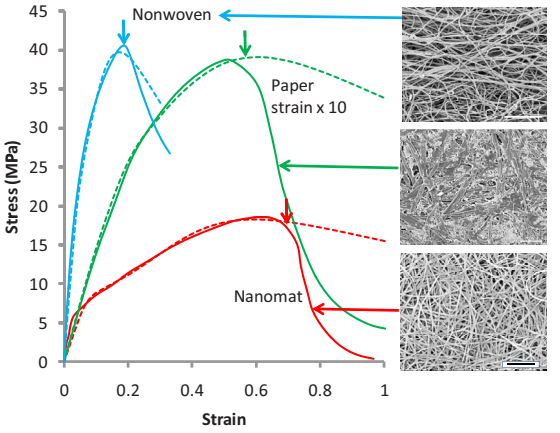

FIG. 6. (Color online) Comparison of model (dashed lines) and observed (solid lines) stress-strain relations for nonwoven fiber materials as labeled, with percolation condition marked as arrows. Scale bar length: 80 g/m^2 office printer paper ("paper") of 100 μm, nonwoven household cleaning cloth ("nonwoven") of 500 μm, and a nanomat scaffold of 10 μm.

at the same value as in the standard stress-strain curve in Fig. 1, indicating that damage is directly linked to strain.

IV. NONWOVEN AND PARTICULATE COMPOSITES

The bonding connectivity in cocoon walls provides an excellent quantitative description of detailed nonlinear mechanical properties in a natural nonwoven composite. However, such a model has limited interest unless it has broader applicability. We noted that a wide range of very different composite materials has stress-strain profiles that have the same form as those of our cocoons while noting also that current models for these materials are mathematically complex, quite narrow in scope, and largely empirical [4–17,29]. Here, too, the main feature shared is the apparent control of mechanical properties by loss of connectivity of bonding between the component materials. Such loss occurs either via fiber-fiber bonding for random fiber or via particle-matrix bonding for particulate composites. Here, we apply the cocoon connectivity model to a range of nonwoven fiber and particulate composites to illustrate how the model can be used with other materials.

A. Nonwovens

Figure 6 compares model and observed stress-strain profiles for the fiber examples of a printer paper, a nonwoven kitchen cloth, and nanomat scaffold [30,31] using physically realistic model parameters listed in Table I.

Nonwoven cloth was purchased from a retailer and is simply a standard household cleaning cloth with a nonwoven structure made from regenerated cellulose fibers, as shown in Fig. 6. The "modulus" parameter values equivalent to fiber strength are 260 MPa, with activation strains of 0.06 and 0.23. These are consistent with properties of Viscose regenerated cellulose fibers with a tensile strength of about 300 MPa and a failure strain of about 8% [32]. The nonwoven structure shows less bending of the fibers relative to cocoons

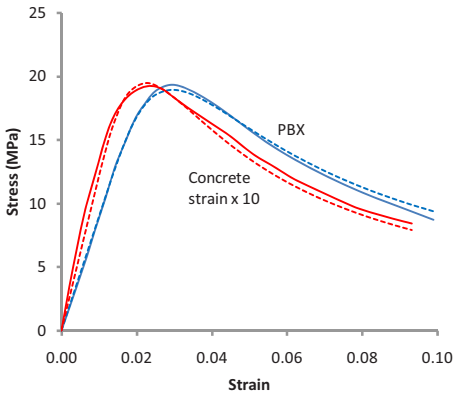

FIG. 7. (Color online) Particulate composites of polymer bonded explosives [34] and concrete [35,36] under compression, which show a single activated process like that in Fig. 2(b). Solid lines for experimental data; dashed lines for model calculations.

with semicircular bends, suggesting a lower value for the upper activation strain for the uncoiling process, relative to 0.6 for cocoons.

Paper samples were taken from a standard office laser printer with a weight of 80 g/m^2 and have low values for activation strains of 0.025 and 0.077, with modulus or component failure stress value of 700 MPa. These strains are due to the noncoiled morphology of the paper fibers, which does not therefore have an upper activation strain for uncoiling. The strength of processed cellulose fibers in the paper could be compared with that for more crystalline Lyocell regenerated cellulose fibers, with a tensile strength of 700 MPa at a failure strain of about 8% [32]. The lower activation strain of 0.025 would then simply be that of the cellulosic binding matrix between the fibers, analogous to the sericin binder matrix in the cocoons.

The nanomat properties were taken from the literature [30,31], and the specific nanomat scaffold was made from dry electrospun poly(lactic-co-glycoic acid) PLGA fibers with fiber diameters in the range of 500–800 nm with a high porosity (92%) structure of highly coiled fibers, which give an upper activation strain comparable with the cocoons at 0.7. The strength of the PLGA polymer fibers is observed to be about 45 MPa [33], in good agreement with the modulus parameter value. The high modulus at very low strain is probably due to strong interfiber hydrogen bonding but has not been included here.

B. Particulate composites

Figure 7 plots stress-strain relations for two important examples of particulate composites as polymer bonded explosive (PBX) [34] and concrete [35,36] under compression. The particulate composites are notably simple in that they have only one activation process for particle-matrix debonding. These composites also show the same form of cyclical loading response as outlined for cocoons above.

For the particulate composites studied in this work so far, they appear to follow a very simple form of the connectivity model with a single-component effect that follows the model equation form very well. In general, particulate composites should follow the standard additivity rules to calculate the composite elastic modulus from their component properties. The main problem comes in calculating the activation strain, ε_a. For the two examples in Fig. 7, we do not know the exact composite composition, so simply demonstrating the form of the model with realistic parameter values is all we can do at this stage. We suggest that debonding between the particles and matrix components follows a fracture mechanics form of debonding stress or strain being dependent upon the size of the particles or, more specifically, the distance between the particles, d. Using an energy equivalence of elastic energy density of modulus, M, inside a cube of side length d with the energy to create six free surfaces with an energy per unit area of $\Gamma \approx 0.15$ J m^{-2}, we can write an expression for the local strain to cavitation, ε_c, with a form [37]

$$\varepsilon_c \approx \sqrt{\frac{12\Gamma}{Md}}. \tag{3}$$

If the volume fraction of rigid particles is ϕ, then the active fraction of matrix in any axis can be approximated as $\phi/3$, such that the tensile strain on the composite to generate the local strain ε_c will be $\varepsilon_c = \phi/3$, which we then equate to the activation strain for loss of bond connectivity in the model as a compressive strain scaled by $1/\nu$, where ν is Poisson's ratio

$$\varepsilon_a \approx \frac{\phi}{3\nu}\sqrt{\frac{12\Gamma}{Md}}. \tag{4}$$

PBX stress-strain curves were taken from literature in the form of experimental data for a standard mock composition 900-21 used at LANL to simulate PBX 9501 [34]. The parameters can be taken in two ways: either they are simply seen as best fit parameters for an excellent fitting function with a modulus of 900 MPa and an activation strain of 3.3% under compression or they can be considered at a more fundamental level as design parameters that need to be quantified in terms of their chemical and morphological composition. By way of illustration for a nonspecific PBX, if we consider 100 μm particles of energetic material with a volume fraction of 0.1 of a binder matrix with a tensile modulus of 2 MPa and a Poisson's ration of 0.5, we can estimate the distance between particles, $d \approx 3.3$ μm, to give an activation strain from Eq. (2) of $\varepsilon_a = 0.035$. The activation strain is in good agreement with the experimental example as a reasonable parameter value with physical relevance.

Concrete is a particulate composite of sand bonded by cement, which is in turn the matrix binder for larger aggregate particles [35]. We again see in Fig. 7 that the model function gives an excellent fit to concrete properties, which are taken from literature [36]. The modulus value of 12 GPa is slightly low for cement and silica materials (20–30 GPa might be expected for silica materials) and the small activation strain of 0.0025 under compression is characteristic of highly brittle silica materials.

Again as a hypothetical example for illustration, consider the concrete example with a modulus of 12 GPa that is a concrete with 25% cement paste with filler modulus of about 30 GPa comprising sand particles with a medium grade par-

ticle size of about 0.2 mm and average separation distance therefore of about 17 μm. The inverse fraction additivity rule for modulus suggests a cement matrix modulus of about 4 GPa. Poisson's ratio of these materials is low at about 0.2. Equation (4) then suggests a compressive activation strain for this model concrete of about $\varepsilon_a \approx 0.0022$, which is a realistic estimate for concrete.

V. CONCLUSION

We conclude that the bioinspired model developed using the highly evolved natural composites of silkworm cocoons provides a physically realistic and quantitative predictive model framework that can be used for analysis, design, or optimization of important new composite materials. The observed mechanism for the loss of stiffness in cocoons is a gradual loss of connectivity of the sericin bonding between load bearing silk fibers. This loss of connectivity can be quantified as a strain-activated fission of the interfiber bonds up to a failure criterion where either a percolation threshold of about 50% of these bonds (quantified as modulus reaching half of its initial value) or the failure stress of the sericin binder is reached, whichever is lower. The connectivity model can be applied to other nonwoven fiber and particulate composites using a small number of physically realistic model parameters.

ACKNOWLEDGMENTS

For funding we thank the AFOSR (Grant No. F49620-03-1-0111) of the USA as well as the European Commission (European Research Council Grant No. SP2-GA-2008-233409), and Chris Holland and Gwilym Davies for taking the photographs.

[1] H. V. Danks, Eur. J. Entomol. **101**, 433 (2004).
[2] H.-P. Zhao, X.-Q. Feng, S.-W. Yu, W.-Z. Cui, and F.-Z. Zou, Polymer **46**, 9192 (2005).
[3] H.-P. Zhao, X.-Q. Feng, W.-Z. Cui, and F.-Z. Zou, Eng. Fract. Mech. **74**, 1953 (2007).
[4] D. H. Page, Tappi J. **52**, 674 (1969).
[5] O. Kallmes, G. Bernier, and M. Perez, Pap. Technol. Ind. **18**, 222 (1977).
[6] C. T. J. Dodson, Rep. Prog. Phys. **33**, 1 (1970).
[7] H. L. Cox, Br. J. Appl. Phys. **3**, 72 (1952).
[8] J. Åström, S. Saarinen, K. Niskanen, and J. Kurkijarvi, J. Appl. Phys. **75**, 2383 (1994).
[9] J. A. Åström, J. P. Makinen, M. J. Alava, and J. Timonen, Phys. Rev. E **61**, 5550 (2000).
[10] L. A. Carlsson and T. Lindström, Compos. Sci. Technol. **65**, 183 (2005).
[11] S. J. I'Anson and W. W. Sampson, Compos. Sci. Technol. **67**, 1650 (2007).
[12] V. I. Räisänen, M. J. Alava, K. J. Niskanen, and R. M. Nieminen, J. Mater. Res. **12**, 2725 (1997).
[13] V. I. Raisanen and H. J. Hermann, Comput. Methods Appl. Mech. Eng. **161**, 103 (1998).
[14] S. J. Eichhorn and R. J. Young, Compos. Sci. Technol. **63**, 1225 (2003).
[15] Ø. W. Gregersen, A. Hansen, and T. Helle, Evaluation of Newsprint Strength and Runnability by Using Weibull Statistics, Progress in Paper Physics Seminar, Vancouver, Canada, 1998, paper D1 (unpublished).
[16] T. Uesaka, M. Ferahi, D. Hristopulos, N. Deng, and C. Moss, The Science of Papermaking, Transactions of the XIIth Fundamental Research Symposium, Oxford, 2001, edited by C. Baker(unpublished).
[17] R. Wathen and K. Niskanen, Paper Web Strength Distributions and Formation, Progress in Paper Physics Seminar, Syracuse, 2002, p. 55 (unpublished).
[18] R. Daw and S. Tonzani, Nature (London) **462**, 425 (2009).
[19] C. Ortiz and M. C. Boyce, Science **319**, 1053 (2008).
[20] D. Porter and F. Vollrath, Adv. Mater. **21**, 487 (2009).
[21] N. L. Nerurkar *et al.*, Nature Mater. **8**, 986 (2009).
[22] X. Fu, D. Porter, and Z. Shao, Macromolecules **42**, 7877 (2009).
[23] F. Vollrath and D. Porter, Appl. Phys. A: Mater. Sci. Process. **82**, 205 (2006).
[24] D. Porter and P. J. Gould, Int. J. Solids Struct. **46**, 1981 (2009).
[25] Z. Shao and F. Vollrath, Nature (London) **418**, 741 (2002).
[26] H. X. Zhu, N. J. Mills, and J. F. Knott, J. Mech. Phys. Solids **45**, 1875 (1997).
[27] L. J. Gibson and M. F. Ashby, Proc. R. Soc. London, Ser. A **382**, 43 (1982).
[28] R. Zallen, *The Physics of Amorphous Solids* (Wiley-VCH, New York, 1998).
[29] Q. S. Xia, M. C. Boyce, and D. M. Parks, Int. J. Solids Struct. **39**, 4053 (2002).
[30] W. J. Li, C. T. Laurencin, E. J. Caterson, R. S. Tuan, and F. K. Ko, J. Biomed. Mater. Res. Part A **60**, 613 (2002).
[31] Z. M. Huang, Y. Z. Zhang, M. Kotakic, and S. Ramakrishna, Compos. Sci. Technol. **63**, 2223 (2003).
[32] W. Gindl and J. Keckes, Compos. Sci. Technol. **66**, 2049 (2006).
[33] L. Wang, Z. Zhang, H. Chen, S. Zhang, and C. Xiong, J. Polym. Res. **17**, 77 (2010).
[34] P. Rangaswamy and R. M. Hackett, WIT Trans. Model. Simul.: Comput. Ballistics **45**, 109 (2007).
[35] D. M. Roy, Science **235**, 651 (1987).
[36] F. C. Caner and Z. P. Bazant, J. Eng. Mech. **126**, 954 (2000).
[37] D. Porter, *Multiscale Modelling of Structural Materials*, Chapter 9 of Multiscale Materials Modelling, edited by Xiao Guo (Woodhead Publishing, Cambridge, UK, 2007).